

See discussions, stats, and author profiles for this publication at: <https://www.researchgate.net/publication/387132154>

Transient Thermal Mapping Utilizing the Sintering of Glass-Ceramics

Article in *Advanced Engineering Materials* · December 2024

DOI: 10.1002/adem.202401585

CITATIONS

0

READS

72

2 authors:



Noah Alexander Burke
Rolls-Royce

8 PUBLICATIONS 2 CITATIONS

[SEE PROFILE](#)



Otto Gregory
University of Rhode Island

137 PUBLICATIONS 2,528 CITATIONS

[SEE PROFILE](#)

Transient Thermal Mapping Utilizing the Sintering of Glass-Ceramics


Noah A. Burke and Otto J. Gregory*

Thermal paints are essential for mapping the surface temperature of gas turbine engine components but can only indicate maximum temperature. A novel transient thermal history sensor that combines the capabilities of a thermocouple with those of a thermal paint is developed here, enabling the retrieval of full thermal history using a “sintering” model. The glassy ceramic thermal paint undergoes a qualitative optical transition due to sintering in response to temperature that is quantified using UV–vis spectroscopy. This provides high-resolution transient temperature measurement ($\pm 6^\circ\text{C}$) when maximum temperature is above its glass transition temperature (T_g) of 563°C and up to 660°C . The glass-ceramic coating exhibits strong adhesion to Inconel 718 substrates due to matched coefficients of thermal expansion. By fabricating similar paints with distinct temperature ranges and placing them in proximity, this approach can significantly reduce the number of thermocouples needed for surface temperature mapping, thereby improving the accuracy of measurements required for engine validation.

1. Introduction

Engine designers are continually striving to improve gas turbine engine efficiency while adhering to strict environmental and safety regulations. Increasing operating temperatures can improve both thermodynamic and fuel efficiency, but if not carefully managed, may compromise safety and longevity. Accurate surface temperature measurements provide engineers with critical data to validate and refine computational fluid dynamics and heat transfer models, offer insights for optimizing cooling systems, and ensure operational safety.^[1] Centrifugal forces and surface temperatures inside the hot section can reach upward of $50,000\text{ g}$ and 1500°C , necessitating the use of materials with sufficient thermomechanical properties such as nickel-based superalloys.^[2–4] Oxidation at elevated temperatures presents an additional challenge, as it can degrade material performance over time.^[5] Due to these extreme operating conditions and exotic refractory materials, instrumentation of engine components demands innovative and unique solutions.

N. A. Burke, O. J. Gregory
Sensors and Surface Technology Laboratory
Department of Chemical Engineering
University of Rhode Island
Kingston, RI 02881, USA
E-mail: ogregory@uri.edu

 The ORCID identification number(s) for the author(s) of this article can be found under <https://doi.org/10.1002/adem.202401585>.

DOI: 10.1002/adem.202401585

1.1. Challenges and Advancements in Surface Temperature Measurements

Thermocouples are considered the benchmark of temperature measurement but are unsuitable for spatial temperature mapping due to their point-measurement.^[6] In contrast, techniques like infrared thermography and optical pyrometry, while capable of mapping temperature fields, are unable to be used routinely due to their line-of-sight requirement and thus substantial and expensive hardware modifications.^[7,8] As a result, thermal paints have emerged as an alternative for capturing broader temperature fields without the need for direct line-of-sight or significant hardware alterations. While useful for mapping temperature fields, traditional thermal paints are limited by their ability to capture only maximum

temperatures, short operational duration, dependence on steady-state conditions, and often provide low-resolution qualitative data.^[9] Additionally, their lack of adhesion to engine components frequently renders them ineffective.^[10,11] Consequently, thermal paints necessitate costly and specialized engine tests that may inaccurately represent genuine operating conditions, leaving significant room for improvements in measurement quality, utility, and efficiency.^[12]

For decades, thermal paints have relied on visual color transitions interpreted by technicians, but recent advances in quantitative analysis have enabled their use for broader temperature ranges and higher resolution.^[13] Methods such as 3D scanning, UV–vis and Fourier transform infrared spectroscopy, have been successful in digitizing color changes, thereby improving measurement accuracy and resolution.^[14–18] While traditional thermal paints have made significant advancements with quantitative techniques, a more innovative class of thermal paints—phosphorescent thermal paints—has emerged, offering operation over larger temperature ranges with better resolution.

Phosphorescent thermal paints utilize changes in luminescent properties to recover temperature information.^[19–23] These coatings offer quantitative temperature measurement up to 1400°C with resolution as high as $\pm 5^\circ\text{C}$ and functionality beyond 60 h. Despite their potential, having been employed in nondedicated engine tests, these coatings are still limited to providing steady-state temperature data.^[10,24] Although transient temperature measurements are possible when combined with on-line optical line-of-sight methods, these readings are severely limited to areas where line-of-sight access exists – a significant drawback compared to traditional thermal paints, which can be

applied more universally.^[25–27] Currently, there exists no thermal paint that can obtain transient temperature measurement without line-of-sight measurement.

1.2. Glass-Ceramics for Surface Temperature Measurement

Glass-ceramics have been previously used for thermal history sensing, offering valuable insight into the health of on-line gas turbines.^[28] Similar to thermal fuses, these paints indicate temperature through changes in color, opacity, and texture, while also providing crude thermal history information by correlating glass microstructure to thermal excursions.^[29] These materials are uniquely suited for high-temperature applications due to their high thermal stability, chemical resistance, and predictable microstructural changes when exposed to varying temperatures.^[30,31] Although temperature gradients can negatively impact material uniformity during sintering processes, they are advantageous in thermal history sensing, as even small gradients induce measurable changes in the material's optical and structural properties.^[32] Therefore, glass-ceramics are particularly useful for detecting minor temperature variations enabling precise thermal mapping. This results in a narrow transition range that is unable to cover the full spectrum of temperatures seen in engine testing. To circumvent this, multiple glass-ceramic thermal paints with differing temperature ranges have been used together in proximity to increase the usable temperature range.^[33,34]

These glass-ceramic paints rely on the sintering of glass particles to correlate microstructural properties with temperature. Sintering kinetics often exhibit logarithmic time dependence and strong exponential temperature dependence, critical for design of experiments.^[35–38] A master sintering curve was developed, based on a combined stage sintering model, to predict densification rates under varying thermal histories, essential for predicting microstructure for ceramic processing.^[39–42] Conversely, thermal history sensing requires an inverse approach, using the final state of the glass-ceramic to recover time–temperature information.

In the present study, we have integrated a glass-ceramic thermal paint with a thermocouple to develop a coating capable of high-resolution, transient temperature measurement without a line-of-sight requirement. The rate at which the thermal paint sinters is a function of time at temperature, resulting in an optical transition that is quantifiable using a UV–vis spectrometer. A thermocouple records the temperature variations and the combined data from both measurements feeds into a transient sintering energy model, yielding time–temperature paths that align with direct thermocouple readings.

This system is particularly valuable for mapping the thermal history of components that are inaccessible and located in the most challenging environments, such as the hot section of gas turbine engines. Precise temperature measurements can maximize efficiency of cooling systems and assist in meeting stringent environmental regulations.^[43] Additionally, thermal mapping has the potential to drive material development, including ceramic matrix composites, and the challenges posed by transient temperatures.^[44] Finally, improved temperature mapping can increase safety by predicting hazardous thermal conditions that exceed safety margins.^[45]

2. Results and Discussion

2.1. Thermal Paint Optical Transition for Temperature Measurement

This thermal paint exhibits a distinct optical transition from opaque white powder to a granular appearance to a black glass when exposed to temperatures beyond its glass transition temperature (T_g), as shown in **Figure 1A**. This transition was attributed to the sintering of glass particles which caused surface pores to form and shrink with increasing temperature. Below T_g , discrete particles scatter light diffusely creating an opaque white appearance. Between T_g and the optical transition temperature (T_o), surface pores form and absorb light progressively darkening the surface. At T_o , the surface pores were optimized for light absorption, as

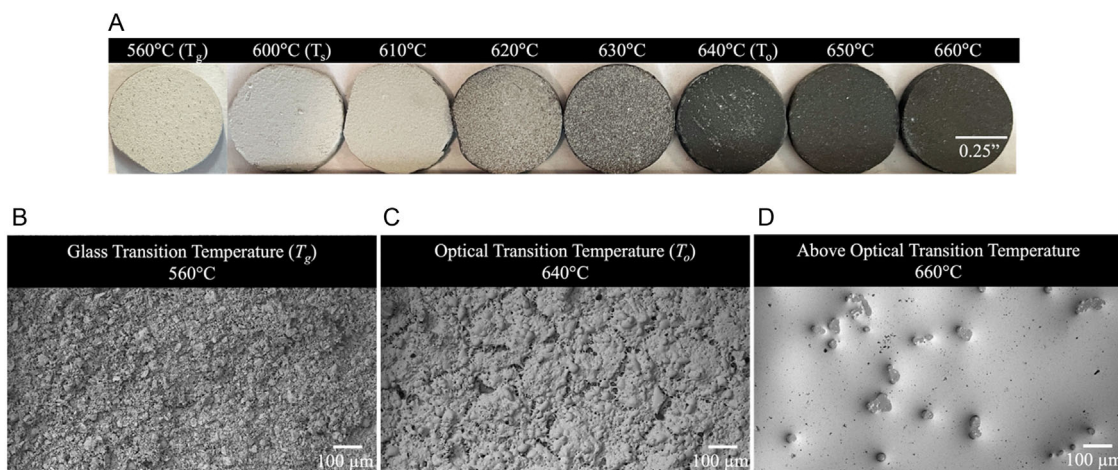


Figure 1. A) Sequential photographs of the thermal paint undergoing an optical transition from an opaque white powder to a black glass after 10 min of exposure to high temperature. SEM micrographs of the thermal paint transition shown at B) the glass transition temperature (T_g), C) optical transition temperature (T_o), and D) above the optical transition temperature.

shown in the scanning electron microscopy (SEM) micrographs of Figure 1B–D.^[33] Beyond T_o , the pores were eliminated and ultimately formed a thin glass film that allowed light to penetrate through the glass coating and reflect off the superalloy substrate. With a narrow transition range of only 60 °C, this paint alone is unsuitable for capturing the full temperature profile required in engine tests. However, fabricating and using multiple paints with different compositions and temperature ranges together could extend the usable range.

Upon examination (Figure 1A), adhesion to the superalloy substrate was facilitated due to similar coefficients of thermal expansion (CTE) between the thermal paint ($8.0 \times 10^{-6} \text{ °C}^{-1}$ between 50 and 500 °C) and the Inconel 718 substrate ($\approx 16 \times 10^{-6} \text{ °C}^{-1}$).^[4,46,47] Despite these differences in values, no thermal paint expansion data were available near the glass transition temperature (T_g) where a significant increase in the CTE was expected that enabled the observed strong adhesion.^[48–50]

Spectroscopic analysis confirmed (and quantified) the thermal paint's optical transition from an opaque white powder to a black glass with high resolution ($\pm 5 \text{ °C}$), as shown in Figure 2A. Understanding the effects of time on sintering and the optical transition is crucial for prolonged temperature calibration. Figure 2B demonstrates the optical transition temperature (T_o) as a function of log time. The results are consistent with multiple viscous flow sintering models and exhibited a logarithmic decay of the optical transition temperature (T_o) and overall transition range over time, which was verified for exposures lasting up to 60 h.^[51,52] Both adhesion and optical properties were maintained throughout this testing period as oxidation was minimized due to the glass powder being already in an oxidized form. Although tests beyond 60 h were not conducted, it is believed the paint would retain its high-temperature properties for longer durations based on the stability observed during the tested time frames. However, further tests will be necessary to confirm its long-term performance.

The thermal paint exposed to different temperatures for varying durations may exhibit identical optical properties, which can lead to inaccurate temperature measurement. This inconsistency

introduces a potential source of error, therefore knowledge of the duration of high-temperature exposure is necessary for accurate measurement. When this factor is accounted for, high-resolution qualitative and quantitative temperature measurements can be obtained over a temperature gradient, agreeing with direct thermocouple measurements, as shown in Figure 3.

Other sources of error can arise from maintaining the correct positioning of the spectrometer probe over the surface of the thermal paint. The probe must be kept at a consistent height and positioned normal to the surface. This becomes more challenging on curved surfaces, such as turbine blades, where deviations in probe distance and angle can introduce inaccuracies. Additionally, as shown in Figure 2A, temperatures at the edges of the optical transition range show higher variance and lower sensitivity in reflectivity and are visually less distinct compared to temperatures near the optical transitioning temperature (T_o).

2.2. Glassy Ceramic Thermal Paint Sintering

The densification of the thermal paint triggers its optical transition as confirmed by optical microscopy, SEM, and UV–vis spectroscopy. Densification (ΔI_0^{-1}) serves as a metric for the extent of sintering (S) and is quantified as a dimensionless value ranging from [0 1], as shown in Figure 4A. During this process, the paint thickness decreased significantly, shrinking from an initial thickness of $\approx 45 \text{ }\mu\text{m}$ to a minimum of $\approx 23 \text{ }\mu\text{m}$ when sintering is complete. Densification data are commonly used to calculate the activation energy of glass-ceramics.^[53–55] During fast-firing sintering, grain growth is suppressed in favor of densification, resulting in two distinct activation energies for these two mechanisms.^[35,56–58] Specifically, the calculated activation energies for the sintering of the glass-ceramic was 696 kJ mol^{-1} during densification, and 235 kJ mol^{-1} during grain growth, as presented in Figure 4B.

Figure 4A confirms that below the transition range, no sintering occurs, resulting in no observable changes. Within the transition range, rapid sintering leads to the optical transition. Above this range, sintering is complete, and no further changes occur.

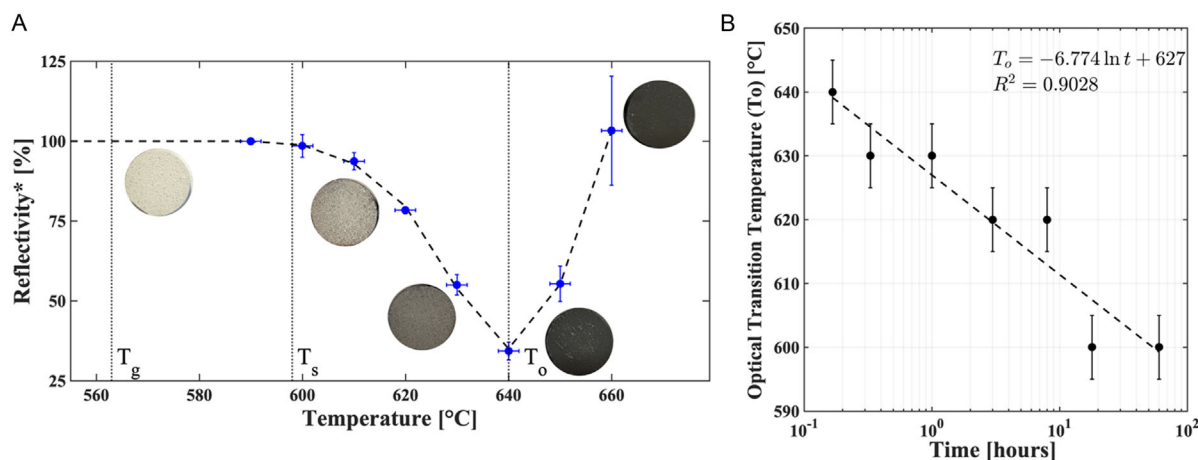


Figure 2. A) Minimum reflectivity in the visible spectrum [380–700 nm] (Reflectivity*) as a function of temperature for 10 min of exposure. Overlaid images illustrate the thermal paint's optical transition, highlighting key temperatures (T_g , T_s , T_o). B) The optical transition temperature (T_o) of the thermal paint as a function of time demonstrates a logarithmic dependence.

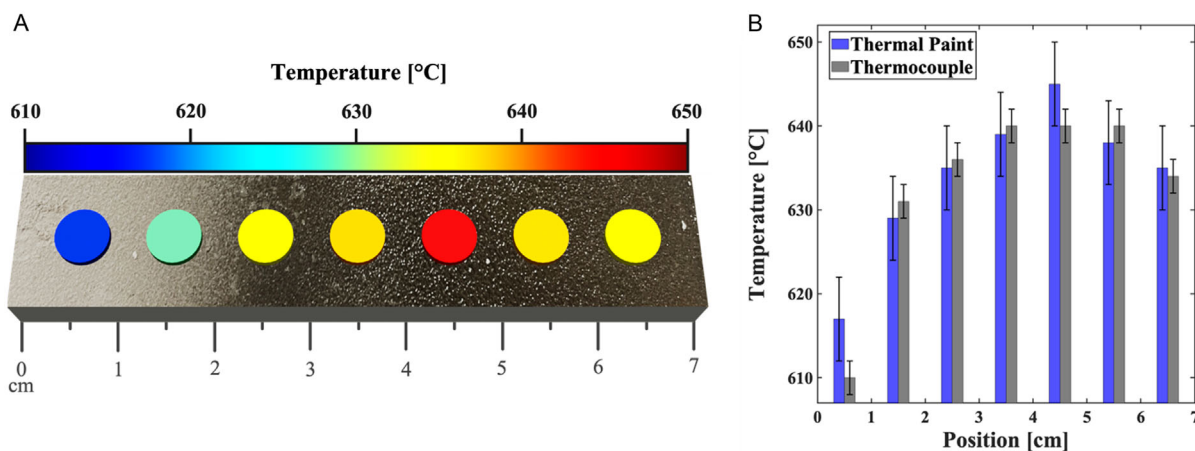


Figure 3. A) Image of the thermal paint exposed to a temperature gradient for 20 min, with UV-vis spectroscopy quantifying the transition for temperature measurement. B) Comparison of the thermal paint's measurement to a type K thermocouple.

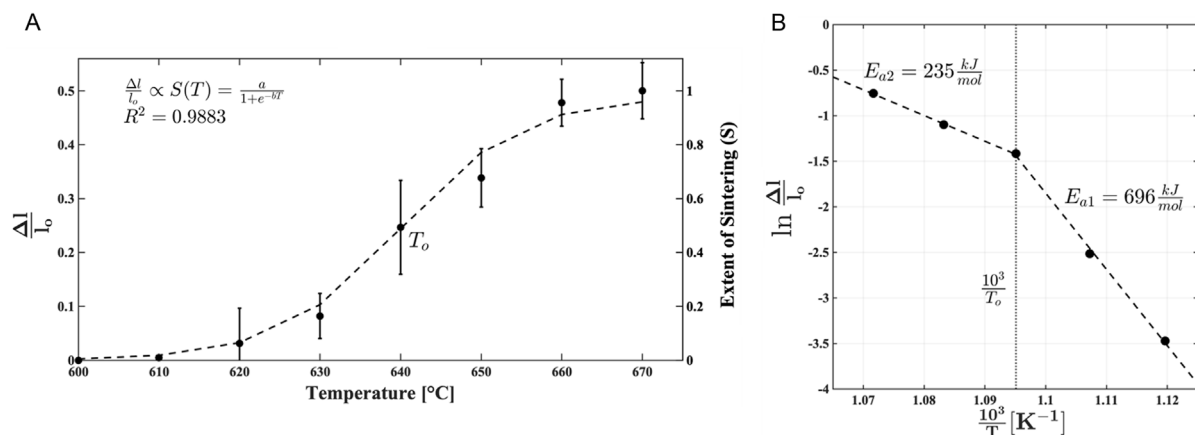


Figure 4. A) Thermal paint densification ($\Delta l/l_0$) and extent of sintering (S) as a function of temperature following 10 min of exposure. B) Arrhenius plot showing the logarithm of densification as a function of inverse temperature to calculate the activation energy of the thermal paint sintering during densification (E_{a1}) and grain growth (E_{a2}).

The optical transition temperature (T_0) corresponds to the inflection point, occurring halfway through the transition where the rate of sintering is maximized and is also referred to as the peak sintering temperature.^[59] This critical temperature marks the point where the rate of grain growth exceeds that of densification.

2.3. Sintering Energy Model to Recover Transient Thermal History

For the thermal paint to function effectively as a thermal history sensor, two key advancements were implemented. First, a thermocouple was strategically placed on the thermal paint to accurately record the temperature path. Here, “temperature path” refers to the shape of the temperature profile as a function of time. Second, a model was formulated to correlate the steady-state temperature data taken from the thermal paint and applied to the transient data from the thermocouple by utilizing densification of the thermal paint as a measure of the extent of sintering.^[34]

Densification is an exponential function of temperature, often modeled using a sigmoidal function.^[60,61] The specific relationship is shown in Equation (1), where parameters a and b are determined from a best fit of the experimental densification data, as determined from Figure 4A.

$$S(T) = \frac{a}{1 + e^{-bT}} \quad (1)$$

Incorporating the effect of time, which can reduce the temperature needed to achieve the same extent of sintering (S), Equation (2) accounts for this effect and influences extent of sintering. Here, c represents the magnitude of the time effect on sintering, as determined in Figure 2B.

$$S(T, t) = \frac{a}{1 + e^{-b(T+c \ln t)}} \quad (2)$$

A method for quantifying sintering by calculating the area under the time–temperature curves is shown in Figure 5A

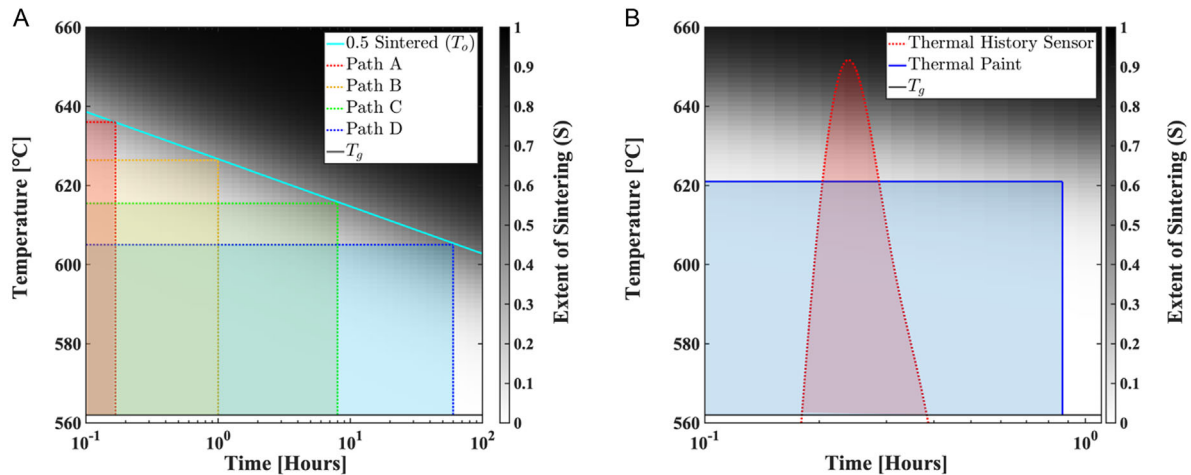


Figure 5. A) Four paths overlayed on the time-temperature-sintering surface each achieving an equal extent of sintering, $S(0.5)$, occurring at the optical transition temperature (T_o), resulting in identical optical properties. B) Results of solving the transient sintering energy equation to equate the steady-state temperature information provided by the thermal paint to the transient information provided by the thermocouple to function as a thermal history sensor.

and as expected, the areas under the sintering curve are unequal.^[59] However, a second, more precise method to quantify the physical states is to calculate the volume under the time-temperature-sintering surface (Equation 2) was used to define the sintering energy (E) in Equation 3.

$$E = R \int_0^t \int_{T_g}^T S(T, t) dT d \ln t \quad (3)$$

where E is sintering energy, R is the universal gas constant, t is time, T is temperature, T_g is the glass transition temperature, and $S(T, t)$ is extent of sintering.

Results from Figure 5A show that all paths that achieve the same extent of sintering (S) also have equal sintering energy (E), making sintering energy a state function, from a thermodynamic perspective (Equation (4)). The key concept here was to equate the steady-state temperature provided by the thermal paint and the temperature path provided by the thermocouple.

$$S_1(T_1, t_1) = S_2(T_2, t_2) \rightarrow E_1 = E_2 \quad (4)$$

To incorporate transient temperature paths, the thermocouple data were normalized to its maximum temperature and fit to a high-order polynomial $T(t)$, a method used to determine duration at peak temperature in the operation of the gas turbine engine.^[62] The sintering energy equation (Equation 3) can be modified to account for transient paths by using the normalized thermocouple path in the upper bound of the temperature integral (Equation 5).

$$E = R \int_0^t \int_{T_g}^{\Phi T(t) + T_i} S(T, t) dT d \ln t \quad (5)$$

where $T(t)$ is the shape of the path, T_i is the initial temperature, and Φ is a scaling parameter to recover the true temperature

path. By solving Equation (5), we equate the steady-state and transient temperature paths that yield the same sintering energy, effectively transforming the thermal paint into a thermal history sensor, as illustrated in Figure 5B.

In summary, the temperature measured from the thermal paint using UV-vis spectroscopy was used to calculate the sintering energy (E). The normalized thermocouple data, $T(t)$, were used as the upper bound of the temperature integral and the scaling parameter (Φ) was varied to satisfy the transient sintering energy equation (Equation (5)). Once the equation is satisfied, the normalized thermocouple data, $T(t)$, were multiplied by a scaling parameter (Φ) to recover the thermal history.

Figure 6 and Table 1 show the results of comparing the thermal history sensor with the thermocouple and thermal paint data used independently for three different temperature paths. The results indicate that the thermal history yields an average temperature within 6 °C of the thermocouple and a more accurate maximum temperature for the paint. However, a critical assumption that underlies this methodology is that the temperature paths of the thermocouple and thermal paint are equal. One potential source of error is that these paths may not align. Therefore, future experiments are necessary to evaluate the validity of this assumption and to investigate its impact on measurement accuracy. However, studies have shown that temperature paths inside gas turbine engines tend to remain unchanged at different locations during operation.^[25–27] Thus, it is best to put the thermocouple or arrays of thermocouples in proximity to one another on the same surface as the thermal paint, where this assumption is more reasonable.^[63–65]

A secondary source of error arises from fitting the normalized thermocouple data to a high-order polynomial. This approach can introduce minor oscillations in the temperature profile, especially when observed at fine resolution, and may lead to significant error if the temperature trajectory is too complex to fit accurately. Future experiments incorporating more complex temperature trajectories and repeated thermal cycling are needed to better simulate real engine testing environments and evaluate

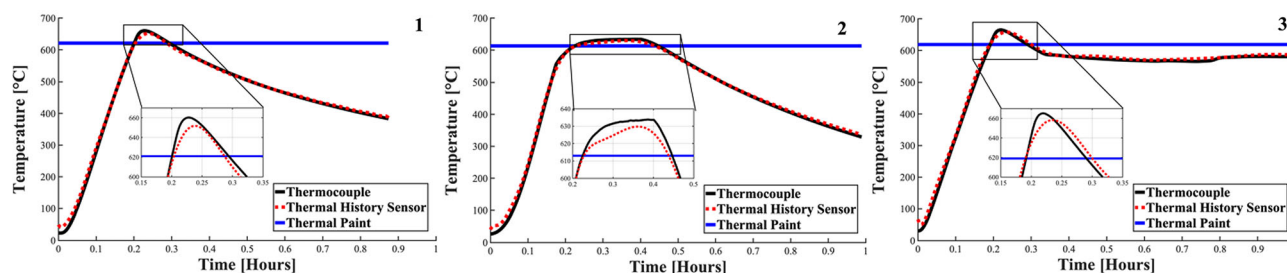


Figure 6. Comparison of thermal history sensor data for three different temperature paths to individual measurements from the thermal paint and thermocouple.

Table 1. Comparison of thermal history sensor data for three different temperature paths to individual measurements from the thermal paint and thermocouple.

Temperature path	Measurement device	Maximum temperature [°C]	Mean error [°C]	Maximum error [°C]
1	Thermocouple	660	–	–
	Thermal history sensor	651	5	27
	Thermal paint	621	172	598
2	Thermocouple	634	–	–
	Thermal history sensor	630	6	24
	Thermal paint	613	160	586
3	Thermocouple	665	–	–
	Thermal history sensor	648	5	36
	Thermal paint	619	73	588

the robustness of this method. Another limitation of using the thermal paint alone, shown in Figure 6, was the tendency to underreport the maximum temperature due to the inability to capture rapid thermal transients or spikes, which is a potential source of error during engine operation. Hence, integrating thermocouples with thermal paint was essential for ensuring accurate, real-time temperature monitoring, especially in transient environments.

3. Conclusion

A glass-ceramic thermal paint was developed such that when paired with a single thermocouple, functions as a transient thermal history sensor. This sensing system provides precise thermal history information with exceptional spatial and thermal resolution achieving temperature accuracy of ± 6 °C. The thermal paint effectively captures maximum temperature when above the glass transition temperature (T_g) of 563 °C and up to 660 °C. It exhibits excellent adhesion to nickel-based superalloys for over 60 h due to its matched thermal expansion coefficient, which is tuned to that of the underlying Inconel 718 substrate. While this temperature range is insufficient to cover the full spectrum required in a gas turbine engine, it could be expanded by using multiple paints in proximity, each with different composition that transition over the desired temperature ranges.

A UV–vis spectrometer has enabled the accurate quantification of the optical transition, facilitating the recovery and digitization of the high-resolution temperature data. A strategically placed thermocouple establishes the temperature path, enabling more comprehensive thermal mapping and more accurate thermal history reconstruction. By utilizing the optical transition of the glassy ceramic to measure the extent of sintering (S) and combining it with normalized thermocouple data along with a sintering energy model, high-resolution transient temperature maps could be produced. These temperature paths align closely with direct thermocouple measurements and show high potential for surface mapping, as opposed to single point measurements.

Implementing this innovative sensing strategy could reduce the number of thermocouples needed for thermal mapping and enhance thermal-spatial resolution, aiding in the development of more comprehensive thermal histories in harsh environments. This approach could provide critical engine performance metrics, validating simulations and optimizing cooling systems and material selection, thus improving engine efficiency, longevity, and safety.

4. Experimental Section

Glass-Ceramic Thermal Paint Preparation: The chemical composition of the thermal paint determines critical properties such as the glass transition temperature (T_g), softening temperature (T_s), and CTE.^[46] A strontium-aluminum glass mixture in powder form (GL-1705) served as the basis of the thermal paint (URI-TP-625), and its composition and properties are listed in Table 2.^[66] The preparation begins by mixing glass powder with methylcellulose and water in the ratio: 5 g glass powder: 3 mL methylcellulose: 1 mL water. This mixture was then shaken vigorously until the desired viscosity was obtained. Inconel 718 coupons 1.3 cm in diameter and 0.32 cm thick were used as the substrates. The surface was prepared by polishing with 125 grit silicon carbide paper, cleaned with isopropyl alcohol, and placed on a hotplate set to 100 °C. The paint was pipetted into a handheld airbrush and sprayed evenly onto the prepared coupons until the surface was completely covered. This resulted in a coating thickness of ≈ 45 μ m. The coupons were then heated in a box furnace and ramped from ambient to 300 °C at a rate of 5 °C min^{−1}. This preliminary heating step served to burnout the binder and promote adhesion to the superalloy substrate.

High-Temperature Thermal Paint Testing: After preparing the samples, baseline measurements were taken using a UV–vis spectrometer (Ocean Optics STS-VIS-L-50-400-SMA), an optical microscope, and a SEM to characterize the initial optical and structural properties of the paint. The painted coupons were then exposed to temperatures between the glass transition temperature (T_g) of 563 and 670 °C in a tube furnace

Table 2. Composition and properties of MOSCI GL-1705 glass powder used in the URI-TP-625 thermal paint.^[66]

Chemical species	wt%
Strontium oxide (SrO)	59.2
Aluminium oxide (Al ₂ O ₃)	25.1
Boron oxide (B ₂ O ₃)	9.26
Nickel oxide (NiO)	4.73
Barium oxide (BaO)	1.61
Calcium oxide (CaO)	0.13
Properties	–
Glass transition temperature (T_g)	$563 \pm 10^\circ\text{C}$
Softening temperature (T_s)	$598 \pm 10^\circ\text{C}$
CTE	$8.0 \times 10^{-6} \text{ }^\circ\text{C}^{-1}$ (50–500 °C)

for durations ranging from 10 min to 60 h. A type K thermocouple was placed onto the painted surface to monitor the temperature, ensuring that this surface remained within $\pm 2^\circ\text{C}$ of the target temperature throughout testing and to track temperature path during transient temperature experiments.

Thermal Paint Optical and Sintering Analysis: After high-temperature exposure, the painted coupons were removed from the furnace, allowed to cool to ambient temperature, and visually inspected for changes in color, opacity, and texture to assess the extent of transition. An optical microscope was used to measure changes in thickness ($\Delta l/l_0^{-1}$) which correlated with a change in density to assess the extent of sintering. The UV–vis spectrometer was employed to characterize the optical transition by analyzing the reflection of incident light off the painted surface. The spectrometer was positioned perpendicular (normal) to the painted surface and held 1 cm above, resulting in a spot size of 0.25 cm². Additionally, SEM was used to observe the surface morphology of the thermal paint to provide insight into the mechanism responsible for the optical transition. For clarity, a flowchart summarizing the

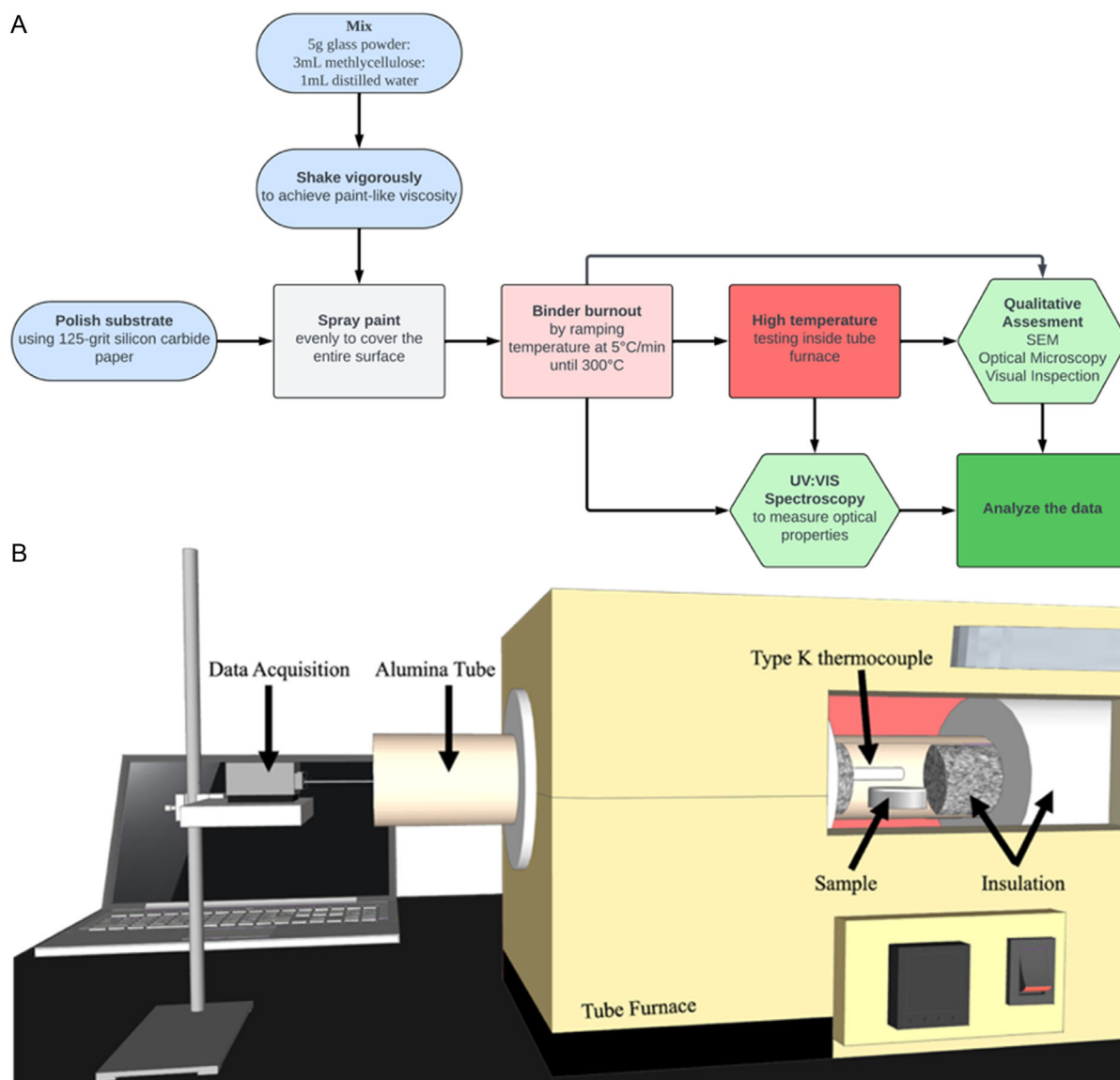


Figure 7. A) Flowchart of the experimental process to fabricate, test, and analyze the thermal paint. B) Illustration of the experimental furnace assembly used to evaluate the performance of the thermal paint, thermocouple, and integrated thermal history sensor.

experimental process, along with an illustration of the furnace assembly used for high-temperature testing is provided in **Figure 7**.

Acknowledgements

This research did not receive any specific grant from funding agencies in the public, commercial, or not-for-profit sectors.

Conflict of Interest

The authors declare no conflict of interest.

Author Contributions

Noah A. Burke: data curation (lead); methodology (equal); software (lead); validation (lead); writing—original draft (lead); writing—review and editing (equal). **Otto J. Gregory:** conceptualization (equal); funding acquisition (lead); resources (lead); supervision (lead); writing—review and editing (equal).

Data Availability Statement

The data that support the findings of this study are available from the corresponding author upon reasonable request.

Keywords

glass transition temperature, glass-ceramics, thermal history sensor, transient temperature mapping, UV–vis spectroscopy

Received: July 5, 2024
Revised: November 26, 2024
Published online:

- [1] S. Naik, J. Krueckels, M. Henze, W. Hofmann, M. Schnieder, presented at *ASME Turbo Expo 2017: Turbomachinery Technical Conf. and Exposition*, Charlotte, NC, USA, June 2017.
- [2] I. Tougas, M. Amani, O. Gregory, *Sensors* **2013**, 13, 15324.
- [3] R. R. Boyer, J. D. Cotton, M. Mohaghegh, R. E. Schafrik, *MRS Bull.* **2015**, 40, 1055.
- [4] A. S. Agazhanov, D. A. Samoshkin, Y. M. Kozlovskii, *J. Phys. Conf. Ser.* **2019**, 1382, 012175.
- [5] M. Zhang, T. Huang, J. Zhang, L. Deng, P. Gong, X. Wang, *Adv. Mater.* **2022**, 34, 2110365.
- [6] S. Liu, Y. Huang, Y. He, Y. Zhu, Z. Wang, *Processes* **2022**, 10, 2528.
- [7] C. Falsetti, M. Sisti, P. F. Beard, *Infrared Phys. Technol.* **2021**, 113, 103574.
- [8] C. Kerr, P. Ivey, *Sens. Rev.* **2004**, 24, 378.
- [9] P. L. Rupesh, M. Arul Prakasajothi, U. Chandrasekhar, R. Mycherla, M. Bhanu Teja, presented at *I-DAD 2018: Innovative Design, Analysis and Development Practices in Aerospace and Automotive Engineering*, Chennai, India, December 2018.
- [10] M. Arulprakasajothi, P. L. Rupesh, *Int. J. Ambient Energy* **2022**, 43, 2324.
- [11] A. J. Neely, H. Riesen, presented at *15th AIAA Inter. Space Planes and Hypersonic Systems and Technologies Conf.*, Dayton, OH, USA, April **2008**.
- [12] D. Peral, A. Zaid, C. Benninghoven, S. Araguas-Rodríguez, D. Kluß, S. Karagiannopoulos, R. Krewinkel, J. Feist, presented at *ASME Turbo Expo 2021: Turbomachinery Technical Conf. and Exposition*, Virtual, ASME, New York, NY, USA June **2024**.
- [13] O. J. Gregory, J. J. McCauley III, US 5135795, **1992**.
- [14] C. Lempereur, R. Andral, J. Y. Prudhomme, *Meas. Sci. Technol.* **2008**, 19, 105501.
- [15] N. Burke, P. Panoutsopoulos, O. J. Gregory, *Int. J. Appl. Glass Sci.* **2023**, 14, 167.
- [16] J. Ge, L. Wang, K. Gui, L. Ye, *Measurement* **2022**, 201, 111741.
- [17] J. Ge, L. Wang, K. Gui, L. Ye, *Measurement* **2023**, 219, 113317.
- [18] A. Kitagawa, C. Welsh, H. Mackilligin, P. Licence, *Appl. Spectrosc.* **2022**, 76, 531.
- [19] A. Rabhiou, J. Feist, A. Kempf, S. Skinner, A. Heyes, *Sens. Actuators A Phys.* **2011**, 169, 18.
- [20] A. L. Heyes, A. Rabhiou, J. P. Feist, A. M. Kempf, in *Volume 1: Aircraft Engine; Ceramics; Coal, Biomass and Alternative Fuels; Controls, Diagnostics and Instrumentation, Proceedings of the ASME Turbo Expo 2012: Turbomachinery Technical Conf. and Exposition*, ASME, Copenhagen, Denmark **2012**, pp. 927–933.
- [21] S. Araguas Rodríguez, T. Jelinek, J. Michálek, Á. Yáñez González, F. Schulte, C. Pilgrim, J. Feist, S. J. Skinner, *J. Glob. Power Propuls. Soc.* **2018**, 2.
- [22] R. Krewinkel, J. Färber, M. Lauer, D. Frank, U. Orth, Á. Y. Gonzalez, C. Pilgrim, J. Feist, R. Saggese, S. Berthier, S. Araguas, in *Volume 5B: Heat Transfer, Proceedings of the ASME Turbo Expo 2016: Turbomachinery Technical Conf. and Exposition*, ASME, Seoul, South Korea, June **2016**.
- [23] W. Cheng, Z. He, N. Ni, Y. Liu, D. Peng, X. Zhao, *J. Lumin.* **2023**, 266, 120281.
- [24] M. Li, H. Cai, P. Wang, W. Cheng, H. Zhang, X. Zhao, D. Peng, *Ceram. Int.* **2024**, 50, 19702.
- [25] J. Feist, Á. Yáñez-Gonzalez, C. Pilgrim, P. Y. Sollazzo, F. Beyrau, A. Heyes, *J. Turbomach.* **2014**, 137.
- [26] J. P. Feist, P. Y. Sollazzo, S. Berthier, B. Charnley, J. Wells, presented at *ASME Turbo Expo 2012: Turbine Technical Conf. and Exposition*, Copenhagen, Denmark, June 2012, pp. 917–926.
- [27] J. P. Feist, P. Y. Sollazzo, S. Berthier, B. Charnley, J. Wells, *ASME J. Eng. Gas Turbines Power* **2012**, 135, 012101.
- [28] G. E. Fair, R. J. Kerans, T. A. Parthasarathy, *Sens. Actuators A Phys.* **2008**, 141, 245.
- [29] M. Trottier, Master's Thesis, University of Rhode Island, **1991**.
- [30] K. C. Nnakwo, F. E. Amadi, V. S. Aigbodion, J. N. Ezeanyanwu, C. C. Nwogbu, A. O. Agbo, E. N. Okigbo, C. C. Daniel-Mkpume, *Int. J. Adv. Manuf. Technol.* **2023**.
- [31] K. C. Nnakwo, F. E. Amadi, C. N. Mbah, *Mater. Res. Express* **2019**, 6, 095202.
- [32] H. Ding, X. Bao, M. Zhang, J. Jin, L. Deng, K. Yao, A. Solouk, P. Gong, X. Wang, *Adv. Powder Mater.* **2023**, 2, 100109.
- [33] P. Panoutsopoulos, Master's Thesis, University of Rhode Island **2022**.
- [34] N. A. Burke, Master's Thesis, University of Rhode Island **2022**.
- [35] S. J. Kim, *Sintering: Densification, Grain Growth, And Microstructure*, Elsevier Butterworth-Heinemann, Amsterdam, New York **2005**, pp. 39–55.
- [36] W. Ku, O. J. Gregory, H. M. Jennings, *J. Am. Ceram. Soc.* **1990**, 73, 286.
- [37] H.-J. Möller, G. Welsch, *J. Am. Ceram. Soc.* **1985**, 68, 320.
- [38] H. L. Juan, Master's Thesis, University of Pittsburgh, **2017**.
- [39] J. D. Hansen, R. P. Rusin, M. Teng, D. L. Johnson, *J. Am. Ceram. Soc.* **1992**, 75, 1129.
- [40] H. Su, D. L. Johnson, *J. Am. Ceram. Soc.* **1996**, 79, 3211.
- [41] T. Frueh, I. O. Ozer, S. F. Poterala, H. Lee, E. R. Kupp, C. Compson, J. Atria, G. L. Messing, *J. Eur. Ceram. Soc.* **2018**, 38, 1030.
- [42] B. Baruah, R. Anand, S. K. Behera, *Ceram. Int.* **2021**, 47, 7253.

- [43] S. Ahsan, T. A. Lemma, M. B. Hashmi, X. Liang, *Meas. Sci. Technol.* **2024**, 35, 18.
- [44] L. S. S. T. Kumar, S. Prajapati, A. K. Mishra, R. S. Mogalapur, H. Garg, *Mechanical Engineering*, Springer, Singapore **2024**.
- [45] N. Abdrakhmanov, Z. Zakirova, M. Guryanova, K. Abdrakhmanova, Y. Savicheva, *IOP Conf. Ser. Earth Environ. Sci.* **2022**, 981, 032047.
- [46] A. Lucia, O. Gregory, *Sci. Rep.* **2023**, 13, 989.
- [47] V. S. Babu, A. S. Pavlovic, M. S. Seehrat, *Superalloys* **1997**, 689.
- [48] P. Lunkenheimer, A. Loidl, B. Riechers, A. Zacccone, K. Samwer, *Nat. Phys.* **2023**, 19, 694.
- [49] J. K. H. Fischer, P. Lunkenheimer, C. Leva, S. M. Winter, M. Lang, C. Mézière, P. Batail, A. Loidl, R. S. Manna, *Phys. Rev. B* **2018**, 97, 235156.
- [50] F. Godey, A. Fleury, A. Soldera, *Sci. Rep.* **2019**, 9, 9638.
- [51] J. Frenkel, *J. Phys.* **1945**, 9, 385.
- [52] M. N. Rahaman, *Ceramic Processing And Sintering*, 2nd Ed, CRC Press, Boca Raton, FL **2003**, pp. 482–512.
- [53] H. Wang, X. Liu, F. Chen, G. Meng, O. T. Sørensen, *J. Am. Ceram. Soc.* **1998**, 81, 781.
- [54] L. D. Silva, A. M. Rodrigues, A. C. M. Rodrigues, M. J. Pascual, A. Durán, A. A. Cabral, *J. Non-Cryst. Solids* **2017**, 473, 33.
- [55] L. Zhang, X. Zhang, H. Zheng, *J. Wuhan Univ. Technol.-Mater. Sci. Ed.* **2018**, 33, 1416.
- [56] S.-J. L. Kang, *Materials* **2020**, 13, 3578.
- [57] D. Xie, L. Wan, D. Song, S. Wang, F. Lin, X. Pan, J. Xu, *Mater. Des.* **2015**, 87, 482.
- [58] D. Sohrabi Baba Heidary, M. Lanagan, C. A. Randall, *J. Eur. Ceram. Soc.* **2018**, 38, 1018.
- [59] M. Stevens, W. M. Carty, *Int. J. Appl. Glass Sci.* **2022**, 13, 620.
- [60] A. Karamanov, B. Dzhantov, M. Paganelli, D. Sighinolfi, *Thermochim. Acta* **2013**, 553, 1.
- [61] Y. Rajkumar, B. M. Rahul, P. Ananth Akash, B. B. Panigrahi, *Int. J. Appl. Ceram. Technol.* **2017**, 14, 63.
- [62] S. Karagiannopoulos, T. Tomoki, D. Peral, S. Araguás Rodríguez, R. Tanaka, J. Hickey, J. P. Feist, *ASME J. Eng. Gas Turbines Power* **2024**, 146, 111005.
- [63] Y. Liu, Q. Yuan, G. Zhu, P. Li, *Shock Vib.* **2018**, 1029520.
- [64] H. Xia, D. Byrd, S. Dekate, B. Lee, *J. Sensors* **2013**, 206738.
- [65] F. J. Dutz, S. Boje, U. Orth, A. W. Koch, J. Roths, *Int. J. Turbomach. Propuls. Power* **2020**, 5, 25.
- [66] N. Burke, P. Panoutsopoulos, Z. Ahlquist, O. J. Gregory, U.S. Patent Application No. US20230365818A1, **2023**